geosciences

MDPI

Article

Contributions to Coastal Flooding Events in Southeast of Vietnam and their link with Global Mean Sea Level Rise

Luis Pedro Melo de Almeida [1,2,*], Rafael Almar [3], Benoit Meyssignac [1] and Nguyen Trung Viet [4]

1 Centre National d'Etudes Spatiales, Laboratoire d'Etudes en Géophysique et Océanographie Spatiales (CNES-LEGOS), 31400 Toulouse, France; benoit.meyssignac@legos.obs-mip.fr
2 Universidade Federal do Rio Grande (FURG), 96203-900 Rio Grande, Brasil
3 Laboratoire d'Etudes en Géophysique et Océanographie Spatiales (IRD-LEGOS), 31400 Toulouse, France; rafael.almar@legos.obs-mip.fr
4 Hanoi Water Resources University, 116705 Hanoi, Vietnam; nguyentrungviet@tlu.edu.vn
* Correspondence: melolp@gmail.com

Received: 8 August 2018; Accepted: 22 November 2018; Published: 26 November 2018

Abstract: This work analyzes the components of the total water level (TWL) that cause flooding in a tropical coastal area (Nha Trang beach, Southeast of Vietnam), and examines their link with global mean sea level rise (GMSLR). Interactions between the wave induced run-up (R) and astronomical tide (AT) were responsible for 43% of the 35 flooding events identified between 1993 and 2015. Most of these events (97%) took place during the winter monsoon season, when long-lasting extreme R and positive non-tidal residual (NTR) are likely to occur. Removal of the GMSLR trend from the NTR was found to affect the flood occurrence of 17% of these events, while the trend in wave height did not have any detectable impact. Our research highlights the direct connection between global climate changes and coastal flooding events.

Keywords: coastal flooding; sea level rise; remote sensing

1. Introduction

Coastlines worldwide are under threat because of climate change [1,2]. Recent probabilistic projections, on the physical basis of climate change [3,4] have projected that the global mean sea level (GMSL) will rise by 0.5 to 1.2 m by the year 2100 under various emissions scenarios because of warming oceans and declining ice volumes. Global mean sea level rise (GMSLR) is already under way and satellite altimetry indicates that sea level has been rising at an average rate of 3.03 ± 0.15 mm/year since 1993 [5]. The impact of GMSLR is not uniform in space and time. Total water level (TWL) at the coast changes differ significantly from GMSL changes because of additional regional and local processes, such as (1) astronomical and meteorological tides, (2) regional sea-level anomalies, and (3) local wave-driven setup and run-up processes [6].

Assessments of coastal vulnerability caused by climate change has tended to focus on the impact of sea-level rise [7], however, recent studies demonstrate that climate-induced variations in the wave climate have the potential to cause coastal impacts (e.g., shoreline retreat and flooding) that are more important than those related to sea-level rise itself [8,9].

Coastal flooding occurs when the TWL exceeds a natural or artificial defence structure (e.g., dune field or seawall), which constitutes the first line of defence of coastal infrastructure [10]. The potential for TWL to exceed these thresholds depends on the relative composition of TWL (interactions between astronomical tides, regional sea levels and wave processes). Recent studies have demonstrated that the dominant contributions differ depending on the time-scales considered [11] and the geographical

location [12]. Variation in the drivers of extreme TWL can also include combinations between components. One study found that the extreme storm "Xaver" caused national-scale impacts on British coastlines due to the highest waves occurring at the same time as spring high tides [13]. The same storm in a different location (German Bight) had a reduced impact because the individual processes (e.g., tides and waves) driving the event did not peak simultaneously [14].

Although it has been studied less, climate-driven contributions to regional and global mean sea levels are very likely to affect the frequency and intensity of coastal flooding events [15]. According to the modelling projections of [16], the frequency of coastal flooding events is likely to increase within a few decades due to GMSLR. Their study suggests that the most affected regions globally will be those with limited water-level variability, i.e., short tailed flood-level distributions, located mainly in the Tropics. Ground-truth validation of these projections has not been performed so far, thus critical testing of the modelled scenarios is required.

The aim of the present work is to investigate the components of TWL which are most influential in driving coastal flooding on a tropical coastal area (Nha Trang coast, Southeast of Vietnam), and examine their link to GMSLR. Using a combination of satellite altimetry and modelled datasets, the TWL from 1993 to 2015 is computed and flooding events identified. The composition of flood-inducing TWL events were analyzed in order to identify the dominant drivers of coastal flooding.

2. Study Site

The coastal site selected for the present work is Nha Trang beach—a sandy beach located within a semi-closed bay in South East Vietnam (Figure 1). The bay is approximately 6 km in length, has an average shoreline orientation NE-SW, and is partially sheltered from south and south-easterly waves by a group of islands. The average beach profile is characterized by a relatively narrow sub-aerial zone (30 m wide), with a steep upper beach face (slope ~0.1) truncated by a seawall (Figure 1c). Note that this coastal region does not suffer from land mass subsidence, due to groundwater extraction, as have other large coastal cities in Vietnam (e.g., Ho Chi Minh City, or Hanoi) [17]. For this reason, land subsidence was not considered in the sea level analysis presented here.

The wave climate and sea level at Nha Trang is strongly influenced by two monsoon seasons—the winter and summer monsoons. The winter monsoon is characterized by strong winds (between 8–12 m/s), energetic waves and positive non-tidal residual (NTR), typically occurring during the wet season (from October to March), while the summer monsoon is characterized by relatively mild wind and wave regimes and small to negative NTR [18,19]. In addition to the monsoon seasons, tropical cyclones, also known as Typhoons, can produce very energetic waves and extreme sea levels in the area, resulting in infrequent but significant coastal flooding events [20]. Nha Trang Bay experiences a mix of diurnal and semi-diurnal tides with a micro-tidal range (maximum range = 1.5 m, during spring tides).

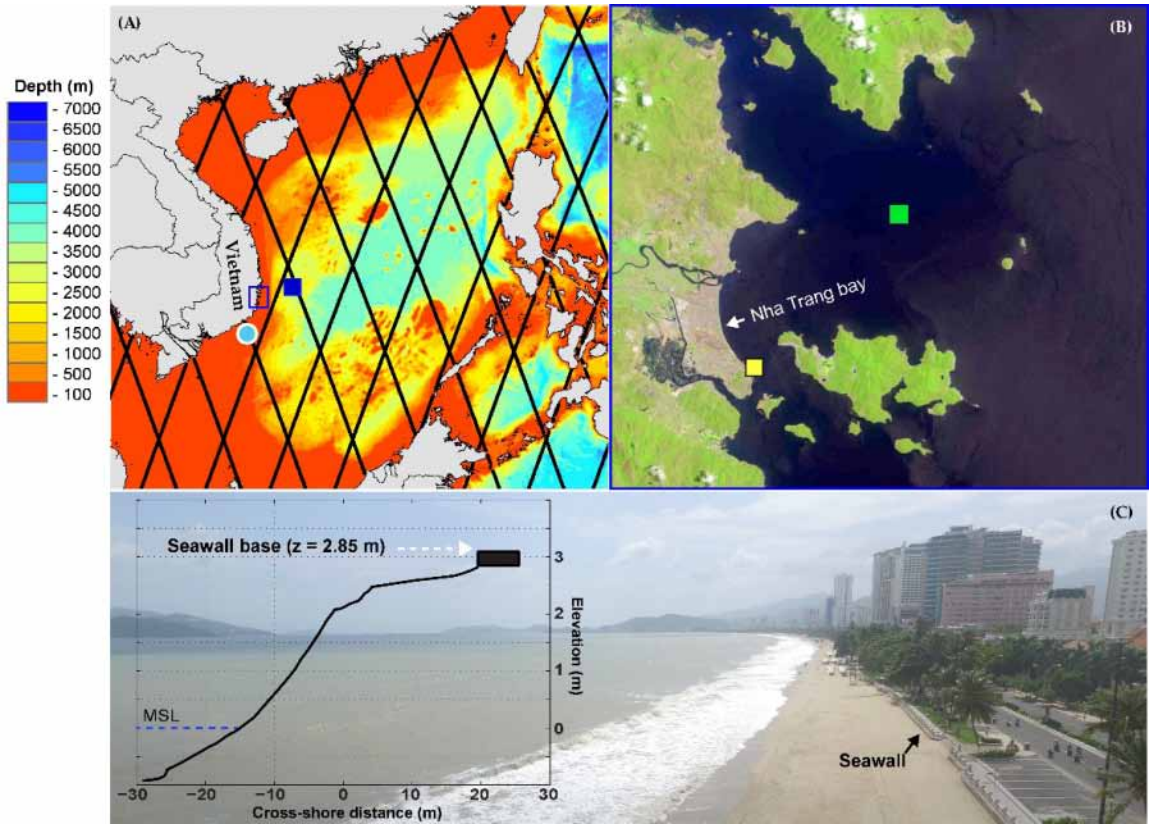

Figure 1. Study site location. (**A**) South China Sea bathymetry indicating the ERA-interim (reanalysis dataset produced by the European Centre for Medium-Range Weather Forecasts—ECMWF) wave grid point (blue filled box), satellite altimetry tracks used to produce the gridded sea-level products (black lines) provided by the Copernicus Marine Environment Monitoring Service (CMEMS), and the location from where altimetric non-tidal residual (NTR) were extracted (blue circle); (**B**) zoom of Landsat image showing the location of Nha Trang Bay and the position of the local tide gauge (yellow box) and the closest tide model grid point (green box); (**C**) view of Nha Trang beach with the location of the seawall and a graph of the average beach profile geometry.

3. Materials and Methods

3.1. Local Sea Level Estimation

The total water level (TWL) at Nha Trang was computed over the 1993–2015 period as:

$$\mathrm{TWL} = \mathrm{NTR} + \mathrm{AT} + \mathrm{R} \quad (1)$$

where NTR is the altimetry non-tidal residual, AT is the astronomical tide and R is the wave-induced vertical run-up. Due to the limited tide gauge observations (2 years of observations—from 1 January 2013 to 8 December 2014), the NTR used in the present work was obtained from satellite altimetry. The satellite altimetry data was obtained from the global ocean SSALTO/DUACS delayed-time level 4 sea surface height products, provided by the Copernicus Marine Environment Monitoring Service (CMEMS). In these products, the along-track data of Topex/Poseidon, Jason-1, Jason-2, Envisat, GFO, ERS-1, ERS-2 and Cryosat-2 were merged and mapped onto a 1/4° grid at a daily resolution. Note that the NTR product is corrected for several atmospheric, oceanographic and meteorological processes (e.g., ionospheric correction, sea-state bias, tide, wind and atmospheric correction; see [21]) The NTR data used in the present work was extracted from the closest point to Nha Trang coast, located at 12.05°N and 109.49°E (Figure 1), and contains information about several non-tidal processes such as storm surges, seasonal and interannual sea level anomalies, and long-term

sea-level rise, from 1993 to 2015. The astronomical tide elevations were obtained from the global tide model Finite Element Solution (FES) [22]. Tide predictions were performed with hourly temporal resolution for a grid point near Nha Trang Bay (Figure 1b). Because there are no records available for R which cover the period 1993–2015, R was estimated using the empirical parameterization of [23], where R is parameterized as a function of deep-water significant wave height (H_s), wave length (L_o), and beach slope (β):

$$R = 1.1\left(0.35\beta\left(H_sL_0\right)^{1/2} + \frac{\left[H_sL_0\left(0.563\beta^2 + 0.004\right)\right]^{1/2}}{2}\right) \quad (2)$$

Wave parameters (H_s and L_o) in Equation (2) were obtained from the 6-hour based ECMWF ERA-Interim wave reanalysis outputs [24] at the grid point closest to Nha Trang Bay (Figure 1b) for the period from 1993 to 2015. The β was defined based on previous field observations at the site [25].

3.2. Validation of the Datasets

TWL components from Equation (1) (NTR and R) were compared with *in situ* observations and evaluated through conventional statistical analysis. The latter consisted of a calculation of the following parameters: (1) correlation coefficient (CC); (2) bias; and (3) root mean squared error (RMSE). The altimeter NTR was compared with the hourly records of the local tide gauge NTR (computed as the difference between the predicted tide and observed tide elevation) for the period of available tide-gauge data (1 January 2013 to 8 December 2014). Before performing these statistical comparisons, wind and dynamic atmospheric corrections (named DAC), which were previously removed from the final product of the altimeter NTR, were re-introduced to include meteorological processes, such as storm surges, in the NTR time series. In addition to this both time series (altimetry and tide gauge datasets) were linearly detrended before the comparison. The predicted tides were harmonically analyzed, and the amplitudes and phases of all constituents were compared with the tidal observations. It was found that the mean amplitude and phase differences were very small (0.001 m and 0.4° respectively) thus the tidal model was preliminarily validated. R estimates (using Equation (2)) were compared with field observations performed by a 2D Lidar during a 5-day field experiment between November and December of 2015 [25]. These field observations were performed under variable offshore wave conditions (varying from energetic to low energy waves) and allowed the quantification of differences in R behavior under changing waves, tides and beach slope conditions [25]. Due to the lack of local wave information (e.g., wave buoy data), the ERA-Interim modelled wave parameters used in Equation (2) were compared to wave information inferred from satellite altimetry. The near-real-time global merged and gridded H_s obtained from SSALTO/DUACS, provided by Copernicus Marine and Environment Monitoring Service (CMEMS), was used for a 3-year (2013 to 2016) comparison with the ERA-Interim H_s. One point near the ERA-Interim output (Figure 1b) was interpolated from the gridded altimeter data (1-day time resolution) to perform this statistical evaluation of the model estimations.

4. Results

4.1. Validation

A comparison between the observations and estimations of the different TWL components is presented in Figure 2. The results show that the altimeter NTR had a good correlation with the local tide gauge NTR (CC = 0.79). It is important to note that the tide gauge NTR used in this comparison was interpolated to the altimeter's temporal resolution (daily), thus some of the short-term tide gauge NTR are not fully captured by the altimeter dataset, as shown in Figure 2a.

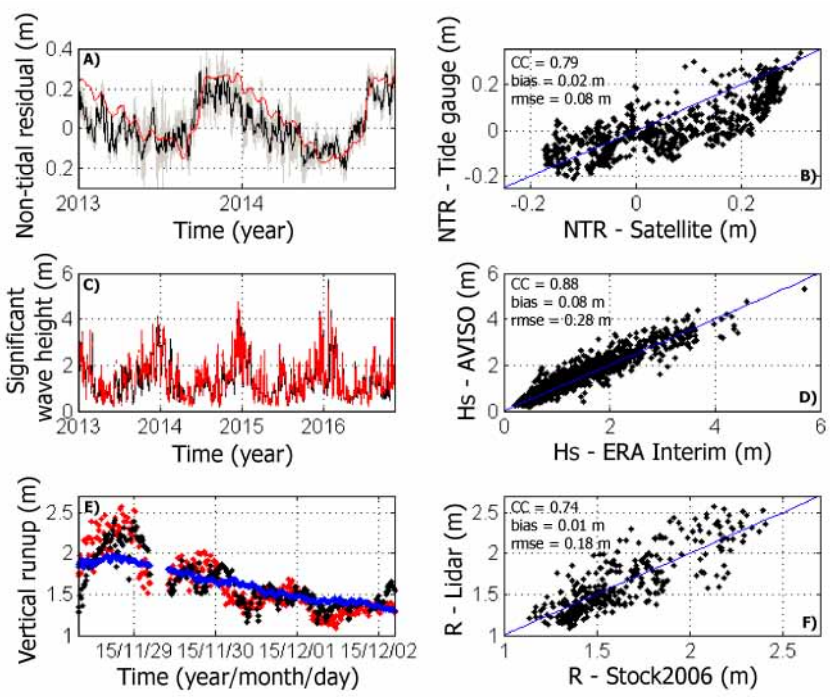

Figure 2. (**A**) time-series of altimetry non-tidal residual (NTR) (black line) and tide gauge NTR (tide gauge 1-day interpolated in red; hourly data in grey); (**B**) non-tidal residual scatterplot; (**C**) time-series of altimeter H_s (red) and ERA-interim H_s (black); (**D**) H_s scatter diagram; (**E**) time-series of Lidar R observations (red dots) and R estimations (with updated beach slope as black dots; fixed beach slope value as blue dots) using the Equation (2); (**F**) R scatterplot.

A comparison between the ERA-interim H_s re-analysis and the satellite H_s observations shows a strong positive correlation (Figure 2d), indicating that the model outputs represent the H_s characteristics in the Nha Trang region. The comparison between the observed and predicted R shows a good agreement (Figure 2e,f), nevertheless the tide modulation of the run-up was improved when beach-slope variations due to the tide were accounted for in Equation (2) (Figure 2e). In order to include temporal variations of beach slope in estimates of R, an empirical relationship between tide and slope was developed: $\beta = 0.037\eta + 0.062$, where η is the tide level (this empirical relationship has CC = 0.76).

4.2. Coastal Flooding Events

The elevation of the top of the seawall (Figure 1) defines the occurrence of coastal flooding events in Nha Trang Bay. Only TWL events that exceeded this threshold were identified as coastal flooding events (CFE). CFEs were validated by comparing the present TWL estimations with local video snapshots (Figure 3—sequence of images). Two tropical storms (October 2013 and December 2014) and one Category 5 Typhoon (Hayian, November 2013) were recorded by the local video camera, and had distinct impacts. The present TWL estimations were accurate for the two tropical storms of December 2014 and October 2013, showing agreement between the estimation and the observed impact (Tropical storm (1) and (2) with no impact and impact, respectively). The impact of the Hayian Typhoon (coastal flooding) was underpredicted by the present TWL estimations (Figure 3). Detailed inspection of the ERA-interim wave time-series during this extreme event showed that it went undetected in model results. This result is similar to that of previous literature [26], which found that regardless of the model's sensitivity to physics, the ERA-interim performs well in predicting Haiyan typhoon's track but substantially underestimates its intensity (the category-5 event was predicted as only category-1).

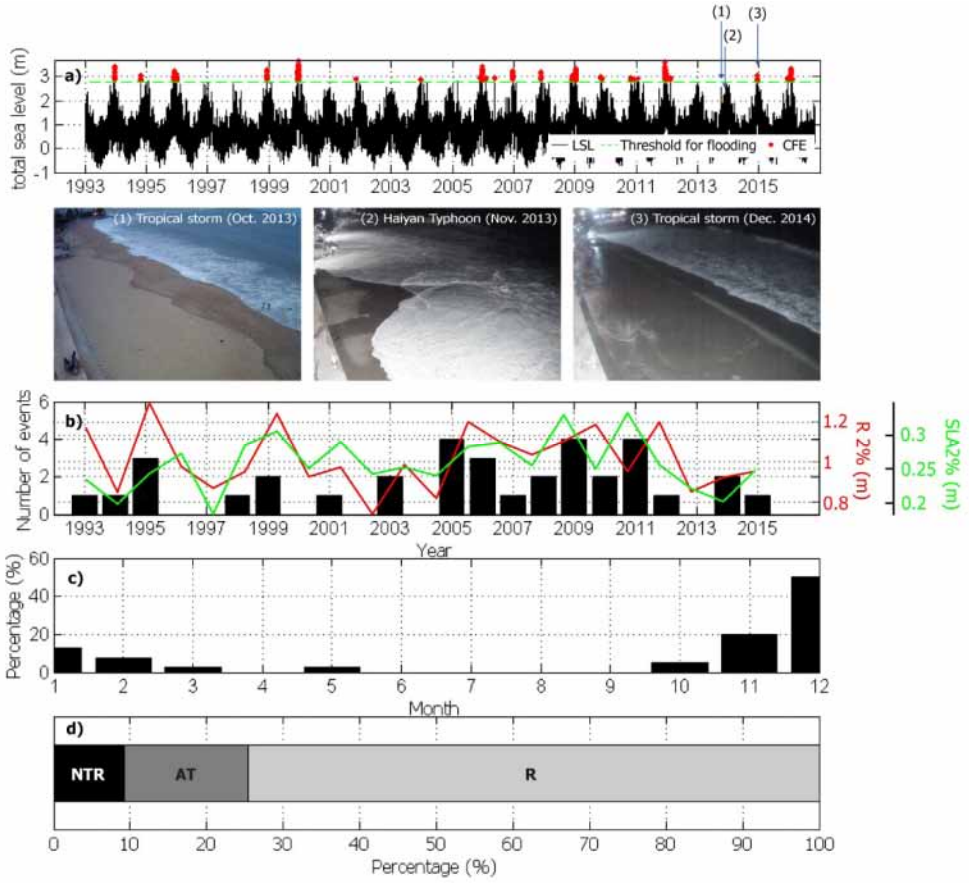

Figure 3. (**a**) Total water level (TWL) time-series indicating the threshold for coastal flooding events (CFE) (dashed green line) and the records that exceeded that threshold (red dots); the blue vertical lines indicate three distinct events where distinct impacts where observed—each number (event) is linked to the field photo in the panel below; the second panel shows three video snapshots of different extreme events recorded locally and used for a qualitative validation; (**b**) number of CFEs per year for the period 1993–2015 with the overlap of the annual 2% of the exceedance of R (R2%; in red) and altimetry NTR (green); (**c**) monthly percentage of occurrence of CFEs showing the main winter monsoon from October (month 10) to March (month 3); (**d**) and the average contribution (%) of the different TWL components to the CFE.

A total of 35 CFEs were identified in the 23-year TWL time-series, the majority of those (97%) occurring during the winter monsoon (October to March), while 3% of them were observed during the summer monsoon (Figure 3b,c). The annual CFE follows the patterns of variability of the R2% particularly well (computed as the 2% of excess of the detrended time series), where CC = 0.76 (Figure 3b). A decomposition of the identified CFE (relative percentage of variance explained by each TWL component; ensemble average for the identified CFEs—Figure 3d) shows that R is the most important component (74.5%), followed by AT (16%) and NTR (9.5%). The importance of the individual TWL components in driving the CFEs was further investigated. By removing R from Equation 1, no event exceeds the flooding threshold, which reinforces the fact that waves are the dominant process governing the CFE in Nha Trang Bay (Table 1). By removing AT, only 5 events occur, and AT combined with R results in 16 events, which represents 46% of the observed events. Hence R and AT combined are the most important interaction driving the CFE. This does not mean that NTR is insignificant; adding NTR to the combination of R and AT results in an additional 19 CFEs.

Table 1. Number of coastal flooding events (CFEs) predicted using different combinations of local sea level (TWL) components.

Components	Number of CFEs
NTR + AT + R	35
NTR + AT	0
NTR + R	5
AT + R	16

4.3. Contributions of Global and Regional Climate Change to Coastal Flooding Events

Trends in the climate-driven components (NTR trend = 4.51 mm/year—computed from altimetric NTR; and R = 1.58 mm/year) were removed and the number of CFEs was re-calculated. Removal of the trend from the NTR dataset reduced the number of events to 29, while the detrended R had no effect on the number of events.

To further investigate the processes underlying the trend in NTR, global and regional climate contributions were removed from the signal. First, the global mean sea level rise (GMSLR) trend (3.03 ± 0.15 mm/year [5]) was removed from the altimetry NTR signal, and CFE was then re-quantified. The detrended NTR signal was further decomposed using multiple variable linear regression in order to quantify the contributions of regional climate modes of variability. The Pacific Decadal Oscillation index (PDO), computed as the low-pass filter (cutoff frequency of 7 years) of Niño 3.4 index, and inter-annual signature of El Niño Southern Oscillation (ENSO), computed as a low-pass filter (cutoff frequency of 1.3 years) of Niño 3.4 index, were used to reconstruct altimetry NTR following the approach proposed by Zhang and Church [27]:

$$\mathrm{NTR} = a_0 + a_1 \mathrm{PDO} + a_2 \mathrm{El\ niño} + \varepsilon_a \quad (3)$$

where a_0 is the intercept, a_1 is the regression coefficient with respect to the PDO, a_2 the coefficient relative to El Niño and ε_a is the residuals. The reconstructed NTR signal by multivariate linear regression (MVLR) had a good correlation with the observed NTR (CC = 0.86) which is due to the fact that PDO and inter-annual El Niño explain most of the decadal and interannual NTR variability in the South China Sea [19]. Removal of the GMSLR trend from NTR results in 29 CFEs. In other words, 17% of CFEs are directly affected by GMSLR (Figure 4). Most of the CFEs affected by the GMSLR occured between 2003 and 2015. By removing PDO and El Niño components from NTR, 36 and 35 CFEs are quantified respectively. The additional CFE event obtained after removing the PDO component relates to a negative peak in NTR in 2005. The same negative peak was observed after removing the El Ñino component from the NTR signal, although in this case one less CFE was quantified in 2010.

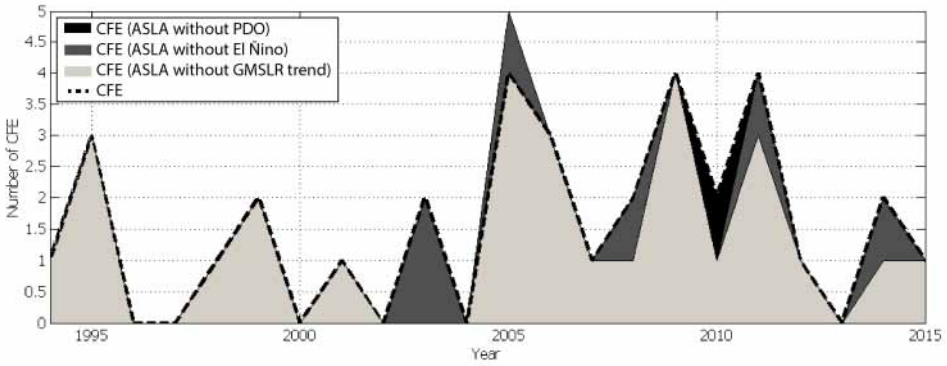

Figure 4. Annual number of CFEs for the period 1993–2015, computed using the raw altimetry NTR time series (black dashed line); other curves indicate the effects of removing the GMSLR trend from the NTR signal (light gray area); removing El Ñino (dark gray area) and PDO (black area) components from the NTR signal.

5. Discussion and Conclusions

This work presents a 23-year time-series of local sea level (TWL) for a coastal site in Southeast Vietnam, using a combination of altimetry and model datasets. The validation process demonstrated that this approach is reliable and adequate for identifying the occurrence and composition of coastal flooding events (CFEs). Nonetheless, it is important to highlight the inaccuracy of the ERA-Interim model in predicting Typhoon strength in the region. Accurate forecasting of tropical cyclone intensity is still a challenge [28,29] and might represent an important limitation in regions where Typhoons are the dominant drivers of coastal flooding. In addition to the waves, very short-term NTR processes, such as storm surges associated with typhoons, are poorly captured by altimetry NTR. The relatively low temporal resolution of altimetry satellites limits the capacity of this remote sensing method to capture this type of short-term sea level change. Nevertheless, along the Nha Trang coast, winter monsoons characterized by long-lasting energetic waves and positive NTR are the main mechanism responsible for shoreline retreat and flooding events [18]. Thus, underestimating the Typhoon contributions is unlikely to significantly affect the present findings.

The wave-driven R was found to be the dominant TWL component driving CFEs at Nha Trang (Figure 3 and Table 1). This result conforms to previous studies of TWL contributions on wave-exposed coastlines [6,11,12] and is likely to be representative of most of the Vietnamese wave-exposed sandy coastlines.

Although our results show that R is the single most important contributor to TWL, it is the interaction between R and other factors that drive coastal flooding in Nha Trang. Interaction between R and AT was found to explain almost half (46%) of the identified CFE occurrences. The majority of the CFEs resulting from this combination occurred during the winter monsoon season, when near-constant energetic wave conditions are observed [18] and there is a higher probability of the simultaneous occurrence of large waves and high tides.

Although NTR was found to have a relatively small individual contribution, by adding it to R + AT, the number of CFEs increases by 54%. Note that the NTR in the South China Sea is also controlled by the monsoon seasons and that long-lasting positive NTRs are typical during winter monsoons [30–33].

Our data show that the altimetry NTR trend was responsible for the occurrence of 6 CFEs (17% of the total number of events). Decomposition of the ASLA signal demonstrated that the GMSLR is the main process responsible for this trend. The PDO and El Ñiño contributions to the NTR signal had a small effect on CFE occurrence. Compared to the 1990 and early 2000s, NTR trends had a greater impact on CFE occurrence from 2003 onwards, coinciding with a period when large NTR and R values where observed. This result suggests that a persistent increment in the base water level is very likely to increase the probability of winter monsoon NTR and R extremes, in turn promoting CFEs at Nha Trang. Considering that the positive NTR trend in the South China Sea is larger than GMSLR [19,34–36], an increase in the number of CFEs is expected in the future, as predicted in the global simulations of Vitousek et al. [16]. These findings highlight the need to assess the composition of the CFE in other regions of the coast of Vietnam, including regions with different wave exposition and coastal morphology (i.e., bathymetry and topography) in order to manage the likely increase in flooding risk.

Author Contributions: Conceptualization, L.P.M.A, R.A. and B.M.; Formal analysis, L.P.M.A.; Funding acquisition, L.P.M.A.; Investigation, L.P.M.A.; Methodology, L.P.M.A.; Resources, N.T.V.; Supervision, R.A. and B.M.; Writing—original draft, L.P.M.A.

Funding: This research was funded by the French government's Centre National d'études Spatiales (CNES) Post-doc grants.

Acknowledgments: The authors of this work would like to thank the CTOH—LEGOS group for support with the altimetric sea-level dataset. This study was conducted using E.U. Copernicus Marine Service Information. The authors would like to thank Simon Connor for the English revision and very useful suggestions.

Conflicts of Interest: The authors declare no conflict of interest.

References

1. Field, C.B.; Barros, V.R.; Dokken, D.J.; Mach, K.J.; Mastrandrea, M.D.; Bilir, T.E.; Chatterjee, M.; Ebi, K.L.; Estrada, Y.O.; Genova, R.C.; et al. *IPCC 2014: Climate Change 2014: Impacts, Adaptation, and Vulnerability. Part A: Global and Sectoral Aspects*; Contribution of Working Group II to the Fifth Assessment Report of the Intergovernmental Panel on Climate Change; Cambridge University Press: Cambridge, UK, 2014; 1132p.
2. Barros, V.R.; Field, C.B.; Dokken, D.J.; Mastrandrea, M.D.; Mach, K.J.; Bilir, T.E.; Chatterjee, M.; Ebi, K.L.; Estrada, Y.O.; Genova, R.C.; et al. *IPCC 2014: Climate Change 2014: Impacts, Adaptation, and Vulnerability. Part B: Regional Aspects*; Contribution of Working Group II to the Fifth Assessment Report of the Intergovernmental Panel on Climate Change; Cambridge University Press: Cambridge, UK, 2014; 688p.
3. Kopp, R.E.; Horton, R.M.; Little, C.M.; Mitrovica, J.X.; Oppenheimer, M.; Rasmussen, D.J.; Strauss, B.H.; Tebaldi, C. Probabilistic 21st and 22nd century sea-level projections at a global network of tide-gauge sites. *Earth Future* **2014**, *2*, 383–406. [CrossRef]
4. DeConto, R.M.; Pollard, D. Contribution of Antarctica to past and future sea-level rise. *Nature* **2016**, *531*, 591–597. [CrossRef] [PubMed]
5. Dieng, H.N.; Cazenave, A.; Meyssignac, B.; Ablain, M. New estimate of the current rate of sea level rise from a sea level budget approach. *Geophys. Res. Lett.* **2017**, *44*, 3744–3751. [CrossRef]
6. Melet, A.; Meyssignac, B.; Almar, R.; Le Gozannet, G. Under-estimated wave contribution to coastal sea-level rise. *Nat. Clim. Chang.* **2018**, *8*, 234–239. [CrossRef]
7. Nicholls, R.J.; Marinova, N.; Lowe, J.A.; Brown, S.; Vellinga, P.; de Gusmão, D.; Hinkel, J.; Tol, R.S. Sea-level rise and its possible impacts given a 'beyond 4 °C world' in the twenty-first century. *Philos. Trans. R. Soc. A* **2011**, *369*, 161–181. [CrossRef] [PubMed]
8. Barnard, P.L.; Short, A.D.; Harley, M.D.; Splinter, K.D.; Vitousek, S.; Turner, I.L.; Allan, J.; Banno, M.; Bryan, K.R.; Doria, A.; et al. Coastal vulnerability across the Pacific dominated by El Niño/Southern Oscillation. *Nat. Geosci.* **2015**, *8*, 801–807. [CrossRef]
9. Harley, M.D.; Turner, I.; Kinsela, M.A.; Middleton, J.H.; Mumford, J.; Splinter, K.D.; Phillips, M.S.; Simmons, J.A.; Hanslow, D.J.; Short, A.D. Extreme coastal erosion enhanced by anomalous extratropical storm wave direction. *Sci. Rep.* **2017**, *7*, 6033. [CrossRef] [PubMed]
10. Almeida, L.P.; Vousdoukas, M.I.; Ferreira, O.; Rodrigues, B.A.; Matias, A. Thresholds for storm impacts on an exposed sandy coastal area in southern Portugal. *Geomorphology* **2012**, *143–144*, 3–12. [CrossRef]
11. Melet, A.; Almar, R.; Meyssignac, B. What dominates sea level at the coast: A case study for the Gulf of Guinea. *Ocean Dyn.* **2016**, *66*, 623–636. [CrossRef]
12. Serafin, K.A.; Ruggiero, P.; Stockdon, H.F. The relative contribution of waves, tides, and non-tidal residuals to extreme total water levels on US West Coast sandy beaches. *Geophys. Res. Lett.* **2017**, *44*, 1839–1847. [CrossRef]
13. Wadey, M.P.; Brown, J.M.; Haigh, I.D.; Dolphin, T.; Wisse, P. Assessment and comparison of extreme sea levels and waves during the 2013/14 storm season in two UK coastal regions. *Nat. Hazards Earth Syst.* **2015**, *15*, 2209–2225. [CrossRef]
14. Dangendorf, S.; Arns, A.; Pinto, J.G.; Ludwing, P.; Jensen, J. The exceptional influence of storm 'Xaver' on design water levels in the German Bight. *Environ. Res. Lett.* **2016**, *11*, 054001. [CrossRef]
15. Wahl, T.; Haigh, I.D.; Nicholls, R.J.; Arns, A.; Dangendorf, S.; Hinkel, J.; Slangen, A.B.A. Understanding extreme sea levels for broad-scale coastal impact and adaptation analysis. *Nat. Commun.* **2017**, *8*, 16075. [CrossRef] [PubMed]
16. Vitousek, S.; Barnard, P.L.; Fletcher, C.H.; Frazer, N.; Erikson, L.; Storlazzi, C.D. Doubling of coastal flooding frequency within decades due to sea-level rise. *Sci. Rep.* **2017**, *7*, 1399. [CrossRef] [PubMed]
17. Thoang, T.T.; Giao, P.H. Subsurface characterization and prediction of land subsidence for HCM City, Vietnam. *Eng. Geol.* **2015**, *199*, 107–124. [CrossRef]
18. Almar, R.; Marchesiello, P.; Almeida, L.P.; Hai, T.D.; Tanaka, H.; Viet, N.T. Shoreline response to a sequence of typhoon and monsoon events. *Water* **2017**, *9*, 364. [CrossRef]
19. Cheng, X.; Xie, S.P.; Du, Y.; Wang, J.; Chen, X.; Wang, J. Interannual-to-decadal variability and trends of sea level in the South China Sea. *Clim. Dyn.* **2016**, *46*, 3113–3126. [CrossRef]

20. Thuan, D.H.; Binh, L.T.; Viet, N.T.; Hanh, D.K.; Almar, R.; Marchesiello, P. Typhoon Impact and Recovery from Continuous Video Monitoring: A Case Study from Nha Trang Beach, Vietnam. *J. Coast. Res.* **2016**, *75*, 263–267. [CrossRef]
21. Birol, F.; Fuller, N.; Lyard, F.; Cancet, M.; Nino, F.; Delebecque, C.; Fleury, S.; Toublanc, F.; Melet, A.; Saraceno, M.; Léger, F. Coastal Applications from Nadir Altimetry: Example of the X-TRACK Regional Products. *Adv. Space Res.* **2017**, *59*, 936–953. [CrossRef]
22. Carrère, L.; Lyard, F.; Cancet, M.; Guillot, A.; Roblou, L. FES2012: A new global tidal model taking advantage of nearly 20-years of altimetry. In Proceedings of the 20 Years of Progress in Radar Altimetry Symposium, Venice, Italy, 24–29 September 2012.
23. Stockdon, H.F.; Holman, R.A.; Howd, P.A.; Sallenger, A.H. Empirical parameterization of setup, swash, and runup. *Coast. Eng.* **2006**, *53*, 576–588. [CrossRef]
24. Dee, D.P.; Uppala, S.M.; Simmons, A.J.; Berrisford, P.; Poli, P.; Kobayashi, S.; Andrae, U.; Balmaseda, M.A.; Balsamo, G.; Bauer, P.; et al. The ERA-Interim reanalysis: Configuration and performance of the data assimilation system. *Q. J. R. Meteorol. Soc.* **2011**, *137*, 553–597. [CrossRef]
25. Almeida, L.P.; Almar, R.; Blenkinsopp, C.; Martins, K.; Benshila, R.; Daly, C. Swash dynamics of a sandy beach with low tide terrace. In Proceedings of the Coastal Dynamics Conference, Helsingør, Denmark, 12–16 June 2017; p. 143.
26. Islam, T.; Srivastava, P.K.; Rico-Ramirez, M.A.; Dai, Q.; Gupta, M.; Singh, S.K. Tracking a tropical cyclone through WRF–ARW simulation and sensitivity of model physics. *Nat. Hazards* **2015**, *76*, 1473–1495. [CrossRef]
27. Zhang, X.; Church, J.A. Sea level trends, interannual and decadal variability in the Pacific Ocean. *Geophys. Res. Lett.* **2012**, *39*, L21701. [CrossRef]
28. Potty, J.; Oo, S.M.; Raju, P.V.S.; Mohanty, U.C. Performance of nested WRF model in typhoon simulations over West Pacific and South China Sea. *Nat. Hazards* **2012**, *63*, 1451–1470. [CrossRef]
29. Osuri, K.K.; Mohanty, U.C.; Routray, A.; Kulkarni, M.A.; Mohapatra, M. Customization of WRF-ARW model with physical parameterization schemes for the simulation of tropical cyclones over North Indian Ocean. *Nat. Hazards* **2012**, *63*, 1337–1359. [CrossRef]
30. Qu, T.; Kim, Y.Y.; Yaremchuk, M.; Tozuka, T.; Ishida, A.; Yamagata, T. Can Luzon Strait transport play a role in conveying the impact of ENSO to the South China Sea? *J. Clim.* **2004**, *17*, 3644–3657. [CrossRef]
31. Qu, T.; Du, Y.; Sasaki, H. South China Sea through flow: A heat and freshwater conveyor. *Geophys. Res. Lett.* **2006**, *33*, L23617. [CrossRef]
32. Cheng, X.; Qi, Y. Trends of sea level variations in the South China Sea from merged altimetry data. *Glob. Planet. Chang.* **2007**, *57*, 371–382. [CrossRef]
33. Du, Y.; Qu, T. Three inflow pathways of the Indonesian through flow as seen from the simple ocean data assimilation. *Dyn. Atmos. Oceans* **2010**, *50*, 233–256. [CrossRef]
34. Li, L.; Xu, J.; Cai, R. Trends of sea level rise in the South China Sea during the 1990s: An altimetry result. *Chin. Sci. Bull.* **2002**, *47*, 582–585. [CrossRef]
35. Fang, G.; Chen, H.; Wei, Z.; Wang, Y.; Wang, X.; Li, C. Trends and interannual variability of the South China Sea surface winds, surface height, and surface temperature in the recent decade. *J. Geophys. Res.* **2006**, *111*, C11S16. [CrossRef]
36. Peng, D.; Palanisamy, H.; Cazenave, A.; Meyssignac, B. Interannual sea level variations in the South China Sea Over 1950–2009. *Mar. Geod.* **2013**, *36*, 164–182. [CrossRef]